Laser and Particle Beams (2005), *23*, 375–383. Printed in the USA.

DOI: 10.1017/S0263034605050536

Bridging the gap between two stream and filamentation instabilities

ANTOINE BRET, MARIE-CHRISTINE FIRPO, AND CLAUDE DEUTSCH
Laboratoire de Physique des Gaz et des Plasmas, Université Paris XI, Orsay, France

(RECEIVED 30 November 2004; ACCEPTED 10 January 2005)

Abstract

We investigate intermediate unstable modes between two stream and filamentation instabilities. We detail the problem of the angle between the wave vector and its electric field and use an electromagnetic formalism allowing for any value for this angle. We display analytical results for 3 different models: cold beam-cold plasma, cold beam-hot plasma and cold relativistic beam-hot plasma. We demonstrate that plasma temperature prompts a critical angle for which waves are unstable at any k and show that for a relativistic beam, the most unstable waves are obtained for wave vectors which are neither normal nor perpendicular to the beam.

Keywords: Fast ignition Scenario; Filamentation Instability; Two-Stream Instability; Weibel Instability

1. INTRODUCTION

Beam plasma interaction plays a crucial role in various fields of physics (Umstadter, 2003). The fast ignition scenario (Mulser and Bauer, 2004; Deutsch *et al.*, 2005) for inertial confinement fusion brought a new interest to the topic. In this scheme, a short impulsion laser produces a relativistic electron beam (Tabak *et al.*, 1994; Koch *et al.*, 1998) which makes its way to the pellet core (Deutsch, 2003; Deutsch *et al.*, 1997) and ignites the Deuterium Tritium fuel. As the beam goes through the plasma, it generates a return current, creating a configuration which is known to undergo both two-stream and Weibel, or filamentation, instabilities. In particular, the later is known to create strong magnetic fields (Okada *et al.*, 1999) within the plasma and filament beam, spreading its energy deposition. Many theoretical, numerical, and experimental works were devoted to the phenomenon and some authors (Tatarakis *et al.*, 2003; Silva *et al.*, 2002) pointed out the need to analyze the coupling between two-stream and filamentation instabilities. Two-stream instability consists in the exponential growth of "longitudinal" modes with wave vector aligned with two counter beams passing through a plasma. On the other hand, Weibel and filamentation instabilities consist in "transverse" unstable modes with wave vector aligned (Weibel, 1959) or normal (Silva *et al.*, 2002) to the beam. Terminology regarding "Weibel" and "filamentation" instabilities is not always accurate as far as the orientation of the wave vector is concerned. In this paper, we shall consider two counter streams passing through a plasma. We shall denote "filamentation" modes unstable transverse waves with wave vector normal to the beam ($\mathbf{k} \perp$ beam, $\mathbf{k} \perp \mathbf{E_k}$), and "Weibel" modes unstable transverse modes with wave vector parallel to the beam ($\mathbf{k} \parallel$ beam, $\mathbf{k} \perp \mathbf{E_k}$).

It then appears that studying the coupling between filamentation and two-stream means studying the coupling between longitudinal and transverse modes. Since two-stream and filamentation unstable modes pertains to the same branch (Godfrey *et al.*, 1975), one sees that some longitudinal unstable modes must evolve continuously to transverse unstable modes when the wave vector orientation gradually changes. This shows that a rigorous investigation of the problem implies dealing with an electromagnetic formalism instead of the longitudinal electrostatic approximation.

These unstable modes with arbitrarily oriented wave vectors usually were investigated using the longitudinal approximation, two-dimensional (2D) fluid models or some mainly numerical approaches (Faĭnberg *et al.*, 1970; Califano *et al.*, 1998). Here we implement a three-dimensional (3D) analytical kinetic approach and focus on these modes. This lets us derive some valid results for any distribution function and analytical ones for specifics functions.

Address correspondence and reprint requests to: Antoine Bret, Laboratoire de Physique des Gaz et des Plasmas, (UMR-CNR 8578), Université Paris XI, Bâtiment 210, Orsay 91405, France. E-mail: antoine.bret@pgp.u-psud.fr

In section 2, we introduce the electromagnetic formalism leading to an expression of the dielectric tensor as well as a general dispersion equation which displays two branches. We then present the three models we shall investigate in the sequel: cold beam-cold plasma interaction, cold beam-hot plasma interaction and finally, cold relativistic beam-hot plasma interaction. We analyze branches 1 and 2 of the dispersion equation in Sections 3 and 4, respectively, before we reach our conclusions.

2. GENERAL ANALYSIS

2.1. Dielectric tensor and dispersion relation

We start from the relativistic Vlasov equation for the electronic distribution function $f(\mathbf{r},\mathbf{p},t)$

$$\frac{\partial f}{\partial t}+\mathbf{v}\cdot\frac{\partial f}{\partial \mathbf{r}}+q\left(\mathbf{E}+\frac{\mathbf{v}}{c}\times\mathbf{B}\right)\cdot\frac{\partial f}{\partial \mathbf{p}}=0, \tag{1}$$

with $\mathbf{v}=\mathbf{p}/(\gamma m)$ and

$$\gamma=\sqrt{1+p^2/(m^2c^2)}=\frac{1}{\sqrt{1-v^2/c^2}}. \tag{2}$$

The mass m will always be the electron mass in the sequel since we shall consider the ions form a fixed background. In the same way, q is the electron charge. One adds Maxwell's equations to the system and the following expression of the dielectric tensor elements is derived (Ichimaru, 1973)

$$\varepsilon_{\alpha\beta}=\delta_{\alpha\beta}+\frac{\omega_p^2}{n_e\omega^2}\int\frac{p_\alpha}{\gamma}\frac{\partial f_0}{\partial p_\beta}d^3p + \frac{\omega_p^2}{n_e\omega^2}\int\frac{p_\alpha p_\beta}{\gamma}\frac{\mathbf{k}\cdot\partial f_0/\partial\mathbf{p}}{m\gamma\omega-\mathbf{k}\cdot\mathbf{p}}d^3p, \tag{3}$$

where the integrals must be evaluated using the standard Landau contour for a proper kinetic treatment. The plasma frequency reads $\omega_p^2=4\pi n_p q^2/m$.

The basic form of the dispersion relation is

$$\frac{\omega^2}{c^2}\,\varepsilon(\mathbf{k},\omega)\mathbf{E}_\mathbf{k}+\mathbf{k}\times(\mathbf{k}\times\mathbf{E}_\mathbf{k})=0, \tag{4}$$

where $\varepsilon(\mathbf{k},\omega)$ is given by (3). If one makes the electrostatic approximation $\mathbf{k}\times\mathbf{E}_\mathbf{k}=0$, the dielectric tensor takes the much simpler form

$$\varepsilon(\mathbf{k},\omega)=1+\frac{4\pi q^2}{k^2}\int\frac{\mathbf{k}\cdot\partial f_0/\partial\mathbf{p}}{\omega-\mathbf{k}\cdot\mathbf{v}}d^3p. \tag{5}$$

Without any assumption upon the nature of the waves, we have $\mathbf{k}\times(\mathbf{k}\times\mathbf{E}_\mathbf{k})=(\mathbf{k}\cdot\mathbf{E}_\mathbf{k})\mathbf{k}-k^2\mathbf{E}_\mathbf{k}$ in Eq. (4) and get

$$\left[\frac{\omega^2}{c^2}\,\varepsilon(\mathbf{k},\omega)+\mathbf{k}\otimes\mathbf{k}-k^2\mathbf{I}\right]\mathbf{E}=\mathbf{0}. \tag{6}$$

Setting

$$\mathbf{T}=\frac{\omega^2}{c^2}\,\varepsilon(\mathbf{k},\omega)+\mathbf{k}\otimes\mathbf{k}-k^2\mathbf{I}, \tag{7}$$

non-trivial ($\mathbf{E}\neq\mathbf{0}$) solutions are obtained provided that $\det(\mathbf{T})=0$, that is,

$$\det\left|\frac{\omega^2}{c^2}\,\varepsilon_{ij}+k_ik_j-k^2\delta_{ij}\right|=0. \tag{8}$$

This forms the most general expression of the dispersion relation. We can now start to detail the geometry of our problem. The velocity distribution anisotropy is set along the z-axis (see Fig. 1 for clarity). Without any restriction of generality, the cylindrical symmetry of the problem allows us to set $\mathbf{k}=(k_x,0,k_z)$. As far as the equilibrium function is concerned, we will use in the sequel electronic distribution functions f_0 such as

$$f_0(\mathbf{p})=f_0(p_x^2+p_y^2,p_z)=f_{0x}(p_x^2)f_{0y}(p_y^2)f_{0z}(p_z), \tag{9}$$

with $\int f_0(\mathbf{p})\,d^3p=n_e$. These distribution functions are isotropic in the (x,y) plane. We can notice that Eq. (9) implies a vanishing average momentum in the (x,y) plane. Under these assumptions, tensors elements $\mathbf{T}_{\alpha,y}$ and $\mathbf{T}_{y,\alpha}$ vanish for $\alpha=x,z$ and Eq. (8) reduces to (with $\eta\equiv\omega/c$)

$$(\eta^2\varepsilon_{yy}-k^2)[(\eta^2\varepsilon_{xx}-k_z^2)(\eta^2\varepsilon_{zz}-k_x^2)-(\eta^2\varepsilon_{xz}+k_zk_x)^2]=0, \tag{10}$$

which displays two branches

$$\eta^2\varepsilon_{yy}-k^2=0\Leftrightarrow\omega=\omega_1(\mathbf{k}) \tag{11}$$

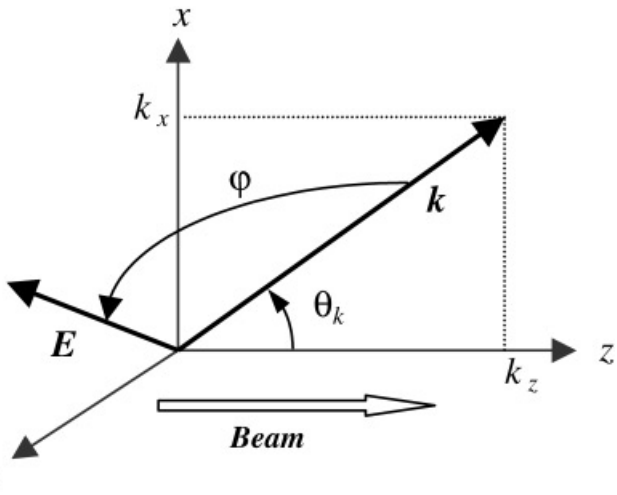

Fig. 1. Geometry of the problem. The angle φ between the electric field $\mathbf{E}$ and the wave vector $\mathbf{k}$ may take all values between 0 and $\pi/2$.

https://doi.org/10.1017/S0263034605050536 Published online by Cambridge University Press

and

$$(\eta^2\varepsilon_{xx} - k_z^2)(\eta^2\varepsilon_{zz} - k_x^2) - (\eta^2\varepsilon_{xz} + k_z k_x)^2 = 0 \Leftrightarrow \omega = \omega_2(\mathbf{k}). \tag{12}$$

These equations are valid for any orientation of the wave vector and any orientation of the electromagnetic field with respect to the wave vector. The first one is a typical dispersion equation for transverse waves. As for the second one, it can be checked, it reduces to an equation for transverse or longitudinal waves when k_x or k_z vanishes. For an arbitrarily oriented wave vector, the angle $(\widehat{\mathbf{k},\mathbf{E}})$ equals the angle between $\mathbf{k}$ and the eigenvector of tensor $\mathbf{T}$ corresponding to the mode investigated.

2.2. Presentation of the three models investigated

In order to detail plasma temperature and relativistic effects on oblique instabilities, we shall now focus on the following three models:

Model 1. The fluid, or cold, approximation, with distribution functions for the beam and plasma given by

$$f_0 = n_p\delta(p_x)\delta(p_y)\delta(p_z + P_p) + n_b\delta(p_x)\delta(p_y)\delta(p_z - P_b). \tag{13}$$

This is the simplest approximation which displays the most basic trend of the phenomenon.

Model 2. The beam is still taken as cold whereas the plasma has a temperature in the direction normal to the beam with distribution function

$$f_0^p = \frac{n_p}{4P_{th}^2}[\Theta(p_x + P_{th}) - \Theta(p_x - P_{th})] \times [\Theta(p_y + P_{th}) - \Theta(p_y - P_{th})]\delta(p_z + P_p). \tag{14}$$

This kind of waterbag distributions was used to derive analytical results in similar situations (Silva *et al.*, 2002; Yoon & Davidson, 1987).

Model 3. Unlike the first two models where we restrict to the non-relativistic regime, here we shall consider relativistic effects together with the distributions functions used in model 2.

As one can see from the functions, we consider no finite size effects. Every model includes a return current which neutralizes the total current (charge neutralization comes from the fixed ions background). One therefore has in every cases $n_p V_p = n_b V_b$ with $P_{p,b} = \gamma_{p,b} m V_{p,b}$ ($\gamma_{p,b} = 1$ for models 1 and 2). We shall make use in the sequel of the dimensionless variables

$$x = \frac{\omega}{\omega_p}, Z = \frac{kV_b}{\omega_p}, \alpha = \frac{n_b}{n_p}, \alpha_t = \frac{V_{th}}{V_b}, \beta = \frac{V_b}{c}, \tag{15}$$

and $\gamma_{p,b} = \sqrt{1 + P_{p,b}^2/(m^2c^2)} = (1 - \beta^2)^{-1/2}$.

Although lengthy, calculations for models 1 and 2 are straightforward. As far as model 3 is concerned, we set $\gamma = 1$ in the integrals involving the plasma distribution function because the two main velocities at stake regarding it are non-relativistic. The first one, the thermal velocity, is about 10 keV in a fusion plasma and remains much smaller than the 0.5 MeV required to tilt relativistic effects. The second velocity, V_p, is the one of the return current induced by the relativistic electron beam with $V_p/c < n_b/n_p = \alpha$. It turns out that within the limits of the fast ignition scenario, α varies from 10^{-1} (plasma edge) to 10^{-3} (plasma core) (Tabak *et al.*, 1994). This shows that the return current velocity is non-relativistic so it is perfectly relevant to restrict relativistic effects to the beam.

3. FIRST BRANCH OF DISPERSION EQUATION

Equation $\varepsilon_{yy} - k^2c^2/\omega^2 = 0$ yields no unstable modes in the first model. On the other hand, the dispersion relation obtained in the third one is (result for model 2 is retrieved through $\gamma_b = 1$)

$$F(x) = P(x) - \frac{1}{3}\frac{\alpha_t^2}{(x/Z + \alpha\cos\theta_k)^2 - (\alpha_t\sin\theta_k)^2}, \tag{16}$$

with

$$P(x) = x^2 - 1 - \frac{\alpha}{\gamma_b} - \frac{Z^2}{\beta^2}. \tag{17}$$

A remarkable feature of this equation is that it still yields unstable modes if one suppresses the beam. Indeed these purely transverse modes were the one investigated in the original Weibel's paper where the system considered was just a plasma characterized by a drifting Maxwellian. Knowing the zeroth order contribution in α to the growth rate will be finite, we just set $\alpha = 0$ in the equation above. Looking for the growth rate under the form $i\delta$ with $\delta \ll 1$, one finds the following expression at any θ_k

$$\delta_{1,\mathbf{k}} \sim \frac{\alpha_t\beta}{\sqrt{3}}\frac{Z}{\sqrt{Z^2 + \beta^2}}\sqrt{1 - \left(\frac{\sin\theta_k}{\sin\theta_c}\right)^2}, \tag{18}$$

with $\sin\theta_c = 1/\sqrt{3}$. Figure 2 shows a numerical evaluation of the growth rate in terms of the reduced wave vector $\mathbf{Z} = \mathbf{k}V_b/\omega_p$. The relative error using Eq. (18) never exceeds 3% so that this formula can be considered as a very good approximation to the growth rate all over the $\mathbf{k}$ space. In terms of the variables k, ω_p, c and V_{th}, the growth rate (18) reads at $\theta_k = 0$ as

$$\delta_{1,0} = \frac{V_{th}}{\sqrt{3}}\frac{k\omega_p}{\sqrt{\omega_p^2 + k^2c^2}}, \tag{19}$$

which, dropping the $1/\sqrt{3}$ factor, is exactly the result already found by Weibel at low k. This is a tribute to the

https://doi.org/10.1017/S0263034605050536 Published online by Cambridge University Press

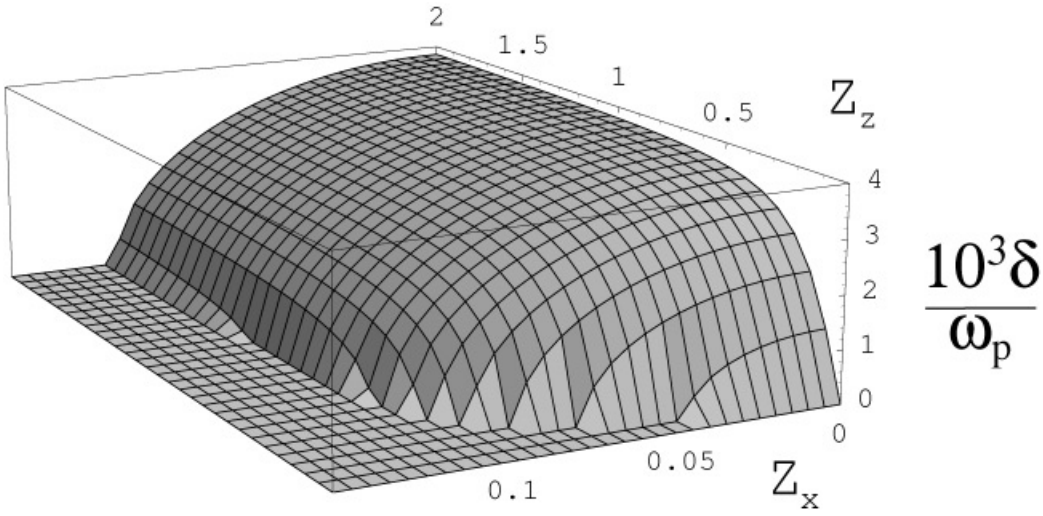

Fig. 2. Numerical evaluation of the first branch growth rate in terms of $\mathbf{Z} = \mathbf{k}V_b/\omega_p$. Parameters are $\alpha_t = \frac{1}{30}$, $\alpha = \frac{1}{10}$ and $\beta = 0.2$. The beam and return current are along the Z_z axis.

interest of the water-bag distribution which is eventually in good agreement with Maxwellian derived results.

4. SECOND BRANCH OF DISPERSION EQUATION: FROM TWO STREAM TO FILAMENTATION

Before we turn to intermediate orientations, we start reviewing known results on both ends of the **k** orientation range. To do so, it is convenient to present results for model 3 since models 1 and 2 are obtained through the $\alpha_t = 0$ and $\gamma_b = 1$ limits, respectively.

4.1. Basic results in the normal and parallel directions

For wave vectors normal to the beam ($\theta_k = \pi/2$, filamentation configuration), one finds a dispersion equation yielding unstable modes for ($\alpha, \alpha_t \ll 1$)

$$Z < \gamma_b \frac{\beta}{\alpha_t}. \tag{20}$$

This is just the non-relativistic result times a factor γ_b so that relativistic effects are destabilizing the system at higher Z's. One also finds an infinite threshold for zero temperature ($\alpha_t = 0$). This is consistent with the known fact that in the fluid model, the growth rate just saturates at high Z. The maximum growth rate in this direction

$$\delta_{m\pi/2} = \beta\sqrt{\frac{\alpha}{\gamma_b}}, \tag{21}$$

is found for $Z \sim \beta/\sqrt{\alpha_t}$. Since $\delta_{m\pi/2} \propto \beta(1-\beta^2)^{1/4}$, the filamentation growth rate reaches a absolute maximum $\delta_{M\pi/2}$ for $\beta = \sqrt{\frac{2}{3}} \sim 0.8$ with

$$\delta_{M\pi/2} = \frac{\sqrt{2}}{3^{3/4}}\sqrt{\alpha}. \tag{22}$$

For wave vectors parallel to the beam ($\theta_k = 0$, two stream configuration), one finds a dispersion equation yielding unstable modes for (Godfrey *et al.*, 1975)

$$Z < 1 + \frac{3}{2}\frac{\alpha^{1/3}}{\gamma_b} \tag{23}$$

in the limit $\alpha \ll 1$. The maximum growth rate

$$\delta_{m0} = \frac{\sqrt{3}}{2^{4/3}}\frac{\alpha^{1/3}}{\gamma_b}, \tag{24}$$

is found at $Z \sim 1$. It worth noticing that the same dispersion Eq. (12) yields these results for wave vectors normal as well as parallel to the beam, describing waves which are transverse on one side and longitudinal on the other (Fig. 3).

4.2. Arbitrary orientation for second branch

We now consider the dispersion Eq. (12) at any θ_k

$$Q(x,\theta_k) = (\eta^2\varepsilon_{xx} - k_z^2)(\eta^2\varepsilon_{zz} - k_x^2) - (\eta^2\varepsilon_{xz} + k_z k_x)^2 = 0. \tag{25}$$

Full expression of dispersion Eq. (25) after inserting the tensor elements (3) is obviously involved. We shall see a

https://doi.org/10.1017/S0263034605050536 Published online by Cambridge University Press

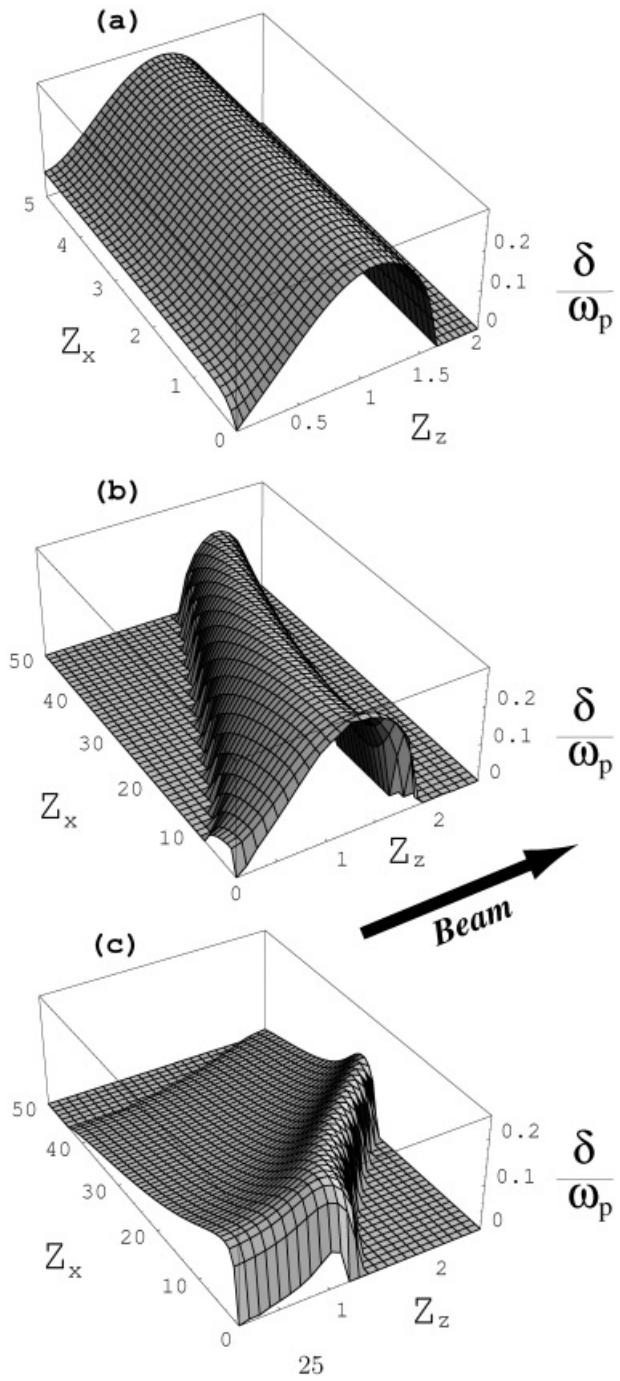

Fig. 3. Numerical evaluation of the two-stream/filamentation growth rate in ω_p units, in terms of $\mathbf{Z} = \mathbf{k}V_b/\omega_p$. (a): model 1 with $\alpha = 0.1$ and $\beta = 0.2$. (b): model 2 with $\alpha = 0.1$, $\alpha_t = \frac{1}{30}$ and $\beta = 0.2$. (c): model 3 with $\alpha = 0.1$, $\alpha_t = \frac{1}{10}$ and $\gamma_b = 5$.

number of analytical conclusions can be reached however. The analysis detailed in the sequel refers to model 2, namely non-relativistic beam-hot plasma interaction. This simplifies exposition and relativistic corrections appear straightforward.

We start noticing that at large x, the asymptotic form of Q must be the dispersion relation at high frequency $(\omega^2 - \omega_p^2 - \omega_b^2)(\omega^2 - \omega_p^2 - \omega_b^2 - k^2c^2) = 0$ so that the polynomial

$$P(x) = (x^2 - 1 - \alpha)(x^2 - 1 - \alpha - Z^2/\beta^2), \tag{26}$$

can be considered as the base of the $Q(x, \theta_k)$ curve, which is just the $P(x)$ curved disturbed by three singularities located at x_1, x_2, and x_3 with (see Fig. 4)

$$\begin{aligned} x_1 &= -Z\alpha \cos\theta_k - Z\alpha_t \sin\theta_k, \\ x_2 &= -Z\alpha \cos\theta_k + Z\alpha_t \sin\theta_k, \\ x_3 &= Z \cos\theta_k. \end{aligned} \tag{27}$$

For $\theta_k = 0$ one has $x_1 = x_2$. When the angle θ_k departs from 0, singularities x_1 and x_2 depart from each other. One has a typical curve such as the one depicted on Figure 4. We have circled the location where real roots may disappear, yielding the instability.

As θ_k keeps increasing, we shall come across a very interesting transition coming from the order of the three singularities defined by Eq. (27). The first one is always negative, and always smaller than the second one since $x_1 = x_2 - 2Z\alpha_t \sin\theta_k$. As for the second and the third one, a brief look shows that $x_2 < x_3$ for small angles but that x_3 is eventually greater than x_2 as the angles approaches $\pi/2$. The inversion occurs for a critical angle ϕ such as $x_2 = x_3$, that is

$$\phi = \arctan \frac{1 + \alpha}{\alpha_t}. \tag{28}$$

This expression is exact and independent of $Z = kV_b/\omega_p$. Due to the singularity located at x_2 and x_3, the local minimum located in between increases when $\theta_k \to \phi$. As a result, one has to increase Z higher and higher to recover two real roots between the singularities. Denoting $Z_c(\theta_k)$ the instability threshold, we see $\lim_{\theta_k \to \phi} Z_c(\theta_k) = \infty$. This feature indicates that the boundary on the stability domain has the cone $\theta_k = \phi$ as an asymptote in the $\mathbf{k}$ space.

The growth rate in the ϕ direction can be evaluated developing the dispersion equation around $x = Z\cos\phi$. In the limit $\alpha, \alpha_t \ll 1$, one finds at high Z (we include relativistic correction)

$$\delta_\phi \sim \beta \sqrt{\frac{\alpha}{\gamma_b}}. \tag{29}$$

This result is exactly the growth rate calculated for $\theta_k = \pi/2$ (see Eq. (21)). Indeed, it can also be derived from a continuity argument. Denoting $\delta^\infty_{\pi/2}$ and δ^∞_ϕ the growth rates at high Z in the $\pi/2$ and ϕ directions, both quantities need to merge for $\alpha_t \ll 1$ since $\lim_{\alpha_t \to 0} \phi = \pi/2$.

Figure 3b displays a numerical evaluation of the growth rate for the two-stream/filamentation mode up to the point (50,3) in the (Z_x, Z_z) plane. This plot confirms the trend we

https://doi.org/10.1017/S0263034605050536 Published online by Cambridge University Press

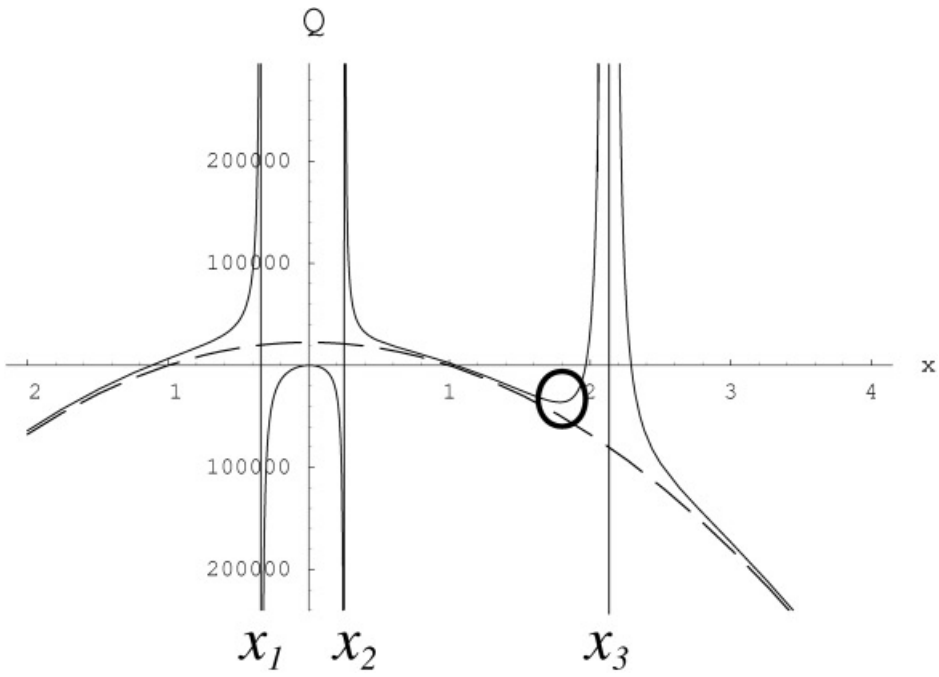

Fig. 4. Plot of $Q(x, \theta_k)$ defined by Eq. (25) as a function of x. Parameters are chosen to display clearly the curve topology with $Z = 15$, $\beta = 0.1$, $\alpha = \alpha_t = \frac{1}{30}$ and $\theta_k = \pi/2.2$. The circle indicates the place where real roots can appear or disappear. The dashed line is the curve of polynomial $P(x)$ defined by Eq. (26).

have already anticipated. One identifies the two-stream instability growth rate along the Z_z axis and the filamentation one along the Z_x axis, but the most remarkable feature on this figure is the non-decreasing growth rate in the ϕ direction.

Figure 3a displays exactly the same plot but for the cold beam interacting with the cold plasma (model 1). There is no such thing as a critical angle here since Eq. (28) yields exactly $\pi/2$ for a cold plasma. Also noticeable is the filamentation saturation at high Z instead of a stabilization.

As mentioned previously, relativistic corrections are straightforward. The first point to emphasize is that the expression of the critical angle evidenced in the non-relativistic case remains unchanged. The origin of this critical angle lies in the dispersion relation singularities x_i (Eq. (27)). The critical angle ϕ is then defined by $x_2 = x_3$ and one easily check it bears no relativistic corrections. We now turn to numerical evaluation all over the wave vector space. We have used fast ignition scenario parameters: a relativistic 2 MeV ($\gamma_b \sim 5$) electron beam with $n_b = 10^{20}$ cm^{-3} entering a 10 keV plasma with $n_p = 10^{21}$ cm^{-3}. This gives $\alpha_t = \frac{1}{25}$ and $\alpha = n_b/n_p = \frac{1}{10}$. Actually, electronic plasma density ranges from 10^{22} to 10^{26} cm^{-3} within this scenario (Tabak *et al.*, 1994) so that α is always smaller than $\frac{1}{10}$. These parameters yield a critical angle $\phi = \pi/2.12$ which is close to the normal direction. Figure 3c displays a numerical evaluation of the growth rate all over the plane (Z_x, Z_z). One notices the long unstable filamentation tail up to $Z_x \sim 40$ in the normal direction, as well as the reduced two stream growth rate in the beam direction. The most striking features are indeed the steady growth rate in the ϕ direction and the maximum reached for $Z_z \sim 1$ and $Z_x \sim 5$. These results are detailed in Figure 5 which is a contour plot of Figure 3c. Note that the angle ϕ between the growth rate's "ridge" and the normal direction is amplified since the largest wave vector shown is $\mathbf{Z} = (50, 2.5)$.

4.3. Maximum growth rate all over the k space

It is obvious from Figure 3c that in the relativistic regime, the maximum growth rate all over the wave vector space is no longer on one axis but rather in between. We now turn to some analytical results concerning the maximum growth rate for any $\mathbf{k}$, in the limit $\alpha, \alpha_t \ll 1$. Hopefully these limits are relevant for most experimental situations where the beam density is much lower than the target one, and the beam velocity much higher than the target thermal velocity.

The position of the maximum growth rate in the $\mathbf{k}$, or $\mathbf{Z}$ space, can be derived from a continuity argument in the $\alpha_t \ll 1$ limit. For a cold plasma the maximum growth rate dependance on Z_x is very weak (see Fig. 3a). The maximum growth rate in the beam direction being always near $Z_z = 1$, we can expect the same value for the Z_z maximum growth rate in the small temperature limit. As for the Z_x component of the maximum, its position coincides with the maximum filamentation growth rate. Having determined which wave vector $\mathbf{Z}_m$ leads to the maximum growth rate in the relativistic regime, we now make use of Figure 6 to find an analytical expression for the corresponding growth rate value $\delta_m(\mathbf{Z}_m)$. An analysis of these plots shows δ_m behaves

https://doi.org/10.1017/S0263034605050536 Published online by Cambridge University Press

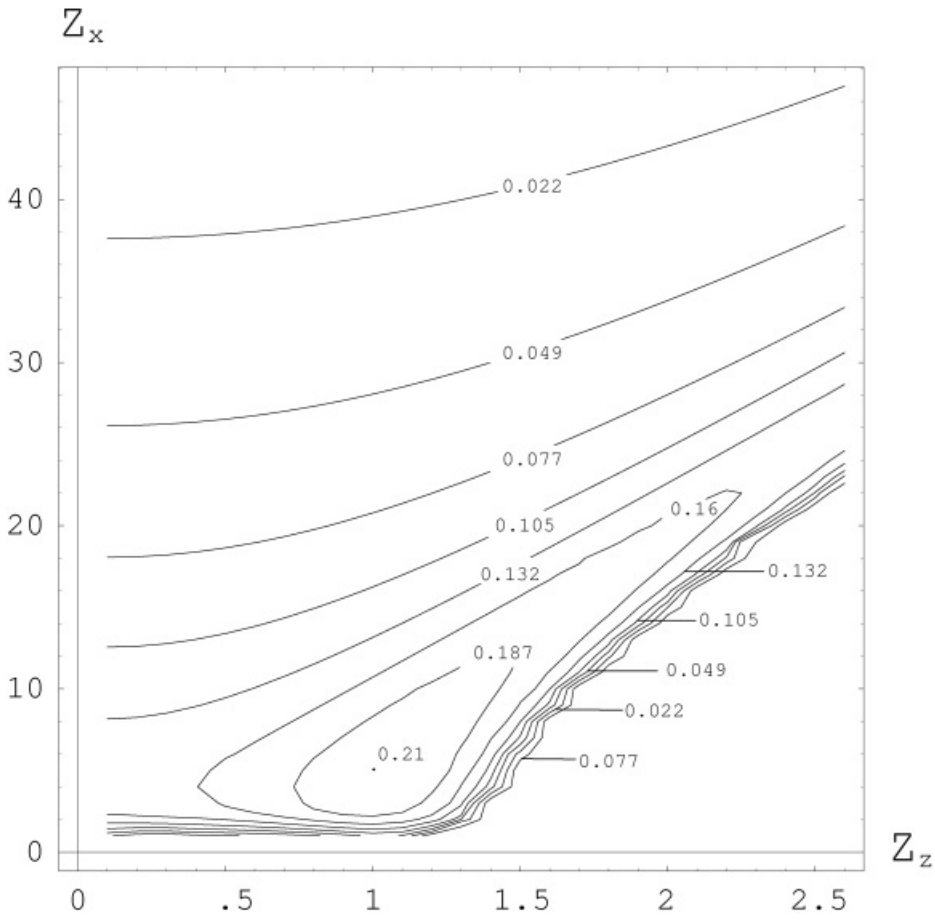

Fig. 5. Contour plot of Figure 3c. Max. growth rate in ω_p units is about 0.21 for $Z_z = 1$ and $Z_x \sim 5.3$ (from Eq. (30)). One sees growth rates values of $0.16\omega_p$ up to $Z_x \sim 25$ in the ϕ direction.

as $\alpha^{1/3}$ for $\alpha \ll 1$ and as $1/\gamma_b^{1/3}$ in the relativistic regime. Figure 6c shows temperature has almost no effect in the small α_t limit so that we can guess $\delta_m(Z_m) \propto (\alpha/\gamma_b)^{1/3}$. For this quantity to join the maximum two stream growth rate for $\gamma_b \sim 1$, the coefficient must be $\sqrt{3}/2^{4/3}$. As a conclusion, the highest growth rate is reached for

$$(Z_{xm}, Z_{zm}) \sim \left(\frac{\beta}{\sqrt{\alpha_t}}, 1\right), \tag{30}$$

with

$$\delta_m(\mathbf{Z}_m) \sim \frac{\sqrt{3}}{2^{4/3}} \left(\frac{\alpha}{\gamma_b}\right)^{1/3}. \tag{31}$$

A result partially displayed in (Faĭnberg *et al.*, 1970). Eq. (30) gives $Z_{xm} = 5.3$ with the parameters used to plot Figure 3c.

As for the transverse or longitudinal character of the waves, a plot of the electric field direction displayed on Figure 7 shows the transition domain between longitudinal two stream waves and filamentation transverse waves extends well bellow the ϕ ridge. A longitudinal wave has its field vector oriented towards the origin of the **Z** space, and one can see on this figure that waves are not longitudinal even for waves vector less oblique than ϕ.

5. DISCUSSION AND CONCLUSION

The interest of working with a fully electromagnetic formalism can easily be measured looking at the filamentation arch contribution to the growth rates plots displayed on Figures 3a, 3b, 3c. Since a purely electrostatic approach yields no filamentation at all, one can see it would fail to describe the picture in model 3. The analysis conducted in this paper unravels in fact two major effects for intermediate wave vector orientations:

1. The existence of a critical angle ϕ for which modes are unstable at any k. Waves in this direction are only approximately longitudinal (see Fig. 7) whereas the asymptotic growth rate is exactly the maximum filamentation growth rate.
2. The presence of the highest unstable mode all over the **k** space out of the main axis. This mode behaves as $1/\gamma^{1/3}$ while filamentation growth rate behaves as $1/\gamma^{1/2}$ and two stream as $1/\gamma$. It is almost longitudinal and dominates the others all the more than γ_b increases.

https://doi.org/10.1017/S0263034605050536 Published online by Cambridge University Press

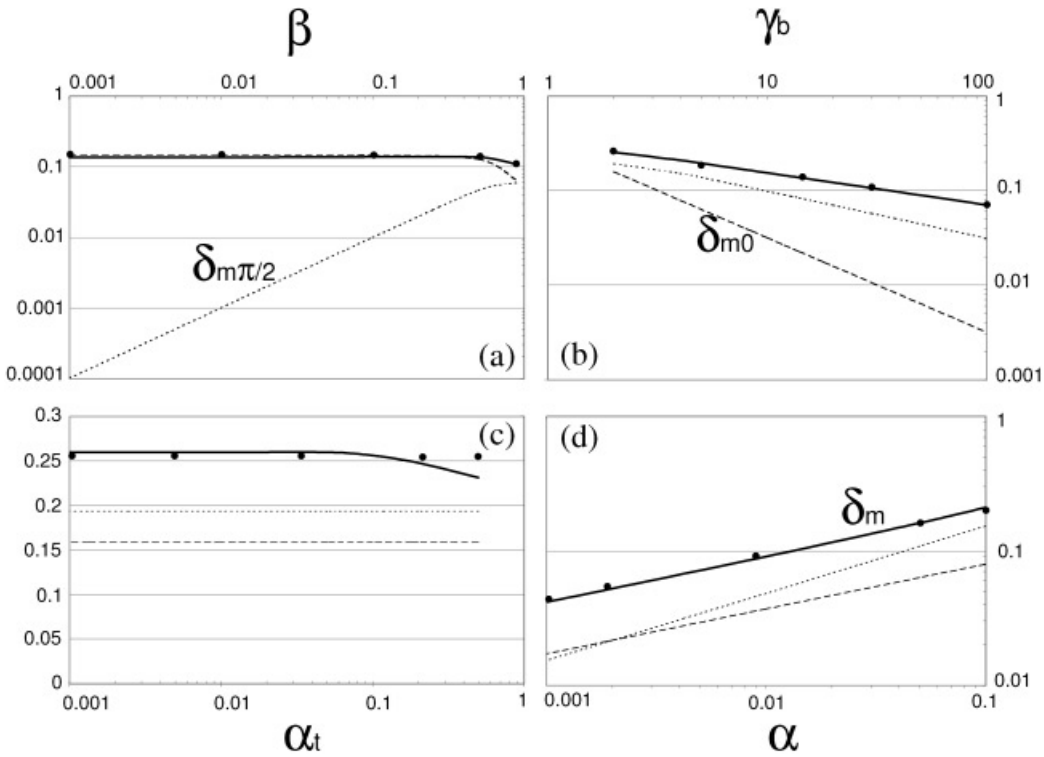

Fig. 6. Comparison between maximum filamentation growth rate ($\delta_{m\pi/2}$, long dashed line), two stream growth rate (δ_{m0}, short dashed line) and the maximum at all $\mathbf{k}$ (δ_m, plain line) in terms of β, γ_b, α_t and α. (a) $\alpha = \frac{1}{10}$, $\alpha_t = \frac{1}{20}$. (b) $\alpha = \frac{1}{10}$, $\alpha_t = \frac{1}{10}$. (c) $\alpha = \frac{1}{10}$, $\gamma_b = 2$. (d) $\gamma_b = 5$, $\alpha_t = \frac{1}{10}$. $\delta_{m\pi/2}$ and δ_{m0} are derived from Eqs. (21, 24) while δ_m is numerically evaluated. Black circles are evaluated from Eq. (31). All growth rates are in ω_p units.

These modes share properties pertaining to two-stream and filamentation modes and can be considered as interpolating between both or them.

The present investigation allows a exhaustive comparison of the various instabilities since the electromagnetic formalism ensures dispersion equation gives every possible unstable modes. In the relativistic regime for example, one must compare two stream/filamentation maximum growth rate δ_m (branch 2) with Weibel growth rate $\delta_{1,0}$ (branch 1, $\mathbf{k} \parallel \mathbf{V}_b$ and $\mathbf{k} \perp \mathbf{E}$). From (18,31), $\delta_{1,0} = \delta_m$ reads (we use the high Z value for $\delta_{1,0}$ and set $\beta \sim 1$)

$$\gamma_b = \frac{27}{16}\frac{\alpha}{\alpha_t^3}. \tag{32}$$

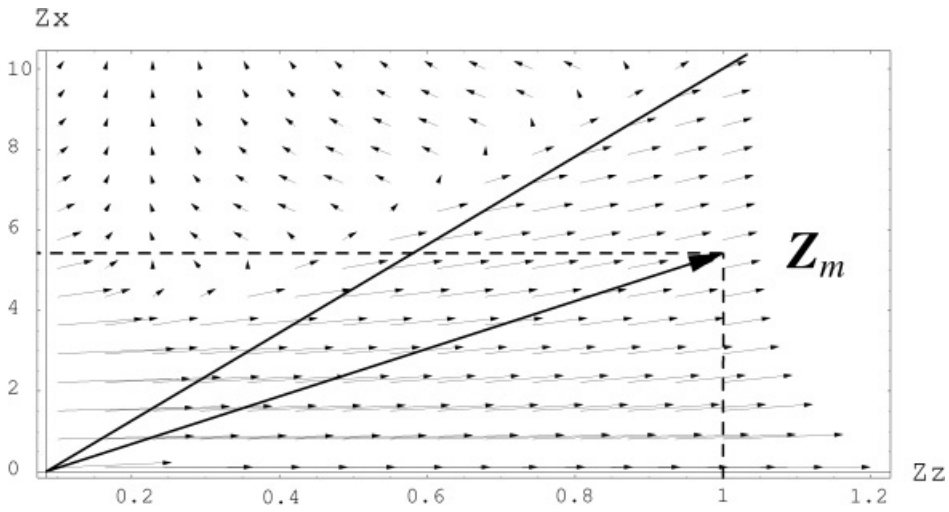

Fig. 7. Direction of the eigenvector electric field $\mathbf{E}(\mathbf{k}, \omega_k)$ for $Z_z < 1$ and $Z_x < 10$ in the cold relativistic beam/hot plasma system. Same parameters as Figure 3c. The plain line indicates the ϕ direction. The arrow represents $\mathbf{Z}_m$, the wave vector yielding the maximum growth rate.

https://doi.org/10.1017/S0263034605050536 Published online by Cambridge University Press

The basic trend of this equation is that Weibel dominates over two stream/filamentation at low beam density, high plasma temperature and high beam energy. However, setting $\alpha_t = \frac{1}{25}$ (10 keV plasma) and $\alpha = \frac{1}{1000}$ yields a very high threshold value $\gamma_b = 26$.

The meaning of the critical angle ϕ can be understood restating Eq. (28) as

$$V_{th} \sin \phi = (V_b + V_p) \cos \phi. \tag{33}$$

A wave with vector making and angle ϕ with the beam "sees" an electron beam (or plasma return current) going at the same velocity than a thermal electron moving in the (x, y) plane. Electrons from both systems can therefore remain in phase with the wave for a number of pulsations and give it energy, according to the wave amplification (or damping) mechanism well explained by Landau (Landau & Lifshitz, 1981).

A further step in the analysis of these mixed two stream/filamentation modes will be to include plasma temperature in every direction and to study transverse beam temperature effects as well.

ACKNOWLEDGMENT

One of us (A. Bret) wishes to thank the Laboratoire de Physique des Gaz et des Plasma for his hospitality.

REFERENCES

Califano, F., Pegoraro, F., Bulanov, S.V. & Mangeney, A. (1998). Kinetic saturation of the weibel instability in a collisionless plasma. *Phys. Rev. E* **57**, 7048.

Deutsch, C. (2003). Transport of megaelectron volt protons for fast ignition. *Laser Part. Beams* **21**, 33–35.

Deutsch, C., Bret, A. & Fromy, P. (2005). Mitigation of electromagnetic instabilities in fast ignition scenario. *Laser Part. Beams* **23**, 5–8.

Deutsch, C., Furukawa, H., Mima, K., Murakami, M. & Nishihara, K. (1997). Interaction physics of the fast ignitor concept. *Laser Part. Beams* **15**, 577.

Fainberg, Y.B., Shapiro, V. & Shevchenko, V. (1970). Nonlinear theory of interaction between a monochromatic beam of relativistic electrons and a plasma. *Soviet Phys. JETP* **30**, 528.

Godfrey, B.B., Shanahan, W.R. & Thode, L.E. (1975). Linear theory of a cold relativistic beam propagating along an external magnetic field. *Phys. Fluids* **18**, 346.

Ichimaru, S. (1973). *Basic Principles of Plasma Physics*. Reading, MA: W.A. Benjamin, Inc.

Koch, J., Back, C., Brown, C., Estabrook, K., Hammel, B., Hatchett, S., Key, M., Kilkenny, J., Landen, O., Lee, R., Moody, J., Offenberger, A., Pennington, D., Ferry, M., Tabak, M., Yanovsky, V., Wallace, R., Wharton, K. & Wilks, S. (1998). Time-resolved x-ray spectroscopy of deeply buried tracer layers as a density and temperature diagnostic for the fast ignitor. *Laser Part. Beams* **16**, 225.

Landau, L.D. & Lifshitz, E.M. (1981). *Course of Theoretical Physics, Physical Kinetics*, New York: Pergamon Press.

Mulser, P. & Bauer, D. (2004). Fast ignition of fusion pellets with superintense lasers: Concepts, problems, and prospectives. *Laser Part. Beams* **22**, 5–12.

Okada, T., Sajiki, I. & Satou, K. (1999). Weibel instability by ultraintense laser pulses. *Laser Part. Beams* **17**, 515.

Silva, L.O., Fonseca, R.A., Tonge, J.W., Mori, W.B. & Dawson, J.M. (2002). On the role of the purely transverse Weibel instability in fast ignitor scenarios. *Phys. Plasmas* **9**, 2458.

Tabak, M., Hammer, J., Glinsky, M.E., Kruer, W.L., Wilks, S.C., Woodworth, J., Campbell, E.M., Perry, M.D. & Mason, R.J. (1994). Ignition and high-gain with ultrapowerful lasers. *Phys. Plasmas* **1**, 1626.

Tatarakis, M., Beg, F.N., Clark, E.L., Dangor, A.E., Edwards, R.D., Evans, R.G., Goldsack, T.J., Ledingham, K.W.D., Norreys, P.A., Sinclair, M.A., Wei, M.-S., Zepf, M. & Krushelnick, K. (2003). Propagation instabilities of high-intensity laser-producted electron beams. *Phys. Rev. Lett.* **90**, 175001.

Umstadter, D. (2003). Relativistic laser-plasma interactions. *J. Phys. D* **36**, 151.

Weibel, E.S. (1959). Spontaneously growing transverse waves in a plasma due to an anisotropic velocity distribution. *Phys. Rev. Lett.* **2**, 83.

Yoon, P.H. & Davidson, R.C. (1987). Exact analytical model of the classical weibel instability in a relativistic anisotropic plasma. *Phys. Rev. A* **35**, 2718.